

Transition to collapsed tetragonal phase in CaFe_2As_2 single crystals as seen by ^{57}Fe Mössbauer spectroscopy

Sergey L. Bud'ko,¹ Xiaoming Ma,^{1,2} Milan Tomić,³

Sheng Ran,^{1,*} Roser Valentí,³ and Paul C. Canfield¹

¹*Ames Laboratory, US DOE and Department of Physics and Astronomy,
Iowa State University, Ames, Iowa 50011, USA*

²*Institute of Applied Magnetism, Key Laboratory for Magnetism
and Magnetic Materials of the Ministry of Education,
Lanzhou University, Lanzhou 730000, Gansu Province, China*

³*Institut für Theoretische Physik, Goethe-Universität Frankfurt,
Max-von-Laue-Straße 1, 60438 Frankfurt am Main, Germany*

(Dated: October 9, 2022)

Abstract

Temperature dependent measurements of ^{57}Fe Mössbauer spectra on CaFe_2As_2 single crystals in the tetragonal and collapsed tetragonal phases are reported. Clear features in the temperature dependencies of the isomer shift, relative spectra area and quadrupole splitting are observed at the transition from the tetragonal to the collapsed tetragonal phase. From the temperature dependent isomer shift and spectral area data, an average stiffening of the phonon modes in the collapsed tetragonal phase is inferred. The quadrupole splitting increases by $\sim 25\%$ on cooling from room temperature to ~ 100 K in the tetragonal phase and is only weakly temperature dependent at low temperatures in the collapsed tetragonal phase, in agreement with anisotropic thermal expansion in this material. In order to gain microscopic insight on these measurements we perform *ab initio* density functional theory calculations of the electric field gradient and the electron density of CaFe_2As_2 in both phases. We show that comparison between calculations and measurements are difficult, but still provide valuable information about the temperature dependent structural details, such as the As- z coordinate, and the bonding properties of the system.

I. INTRODUCTION

CaFe_2As_2 is conceivably one of the most interesting materials in the family of Fe-As based superconductors with a very fragile ground state and extreme sensitivity to the external pressure and/or strain. At ambient pressure, a clear, sharp first order transition at ~ 170 K from high temperature tetragonal - paramagnetic phase to low temperature orthorhombic - antiferromagnetic phase was observed in thermodynamic, transport and microscopic measurements, in single crystals grown out of Sn flux.¹⁻⁶ Under pressure, this transition is initially suppressed at a rate of 10-15 K/kbar^{5,7-11}. As the pressure increases, at about 3 kbar, a paramagnetic - collapsed tetragonal (cT) phase terminates the lower pressure orthorhombic - antiferromagnetic phase near 100 K. The cT transition temperature increases under pressure and reaches 300 K at ~ 15 kbar.⁷⁻⁹ The uniaxial pressure derivatives of the structural/magnetic transition are large and of different signs.¹² The pressure - temperature phase diagram for CaFe_2As_2 is very sensitive to non-hydrostaticity of the applied pressure.^{5,10,13,14}

This extreme sensitivity of pure, as well as substituted CaFe_2As_2 single crystals to external stresses and strains yields an unexpected result: by a judicious choice of the annealing temperature and time (e.g. by control of internal stress fields via nanoscale precipitates) we can tune the structural/magnetic transition temperature in FeAs grown CaFe_2As_2 crystals in a manner similar to application of pressure: suppressing the antiferromagnetic/orthorhombic transition by over 70 K and furthermore, we can obtain the crystals with the cT ground state at ambient pressure.¹⁵ By adding transition metal substitution as an extra parameter, we can tune the ground state of the $\text{Ca}(\text{Fe}_{1-x}\text{T}_x)_2\text{As}_2$ ($\text{T} = \text{Co}, \text{Ni}, \text{Rh}$) crystals to be orthorhombic - antiferromagnetic, tetragonal - superconducting, tetragonal - paramagnetic, and collapsed tetragonal - paramagnetic, all at ambient pressure.^{16,17} Pressure measurements on Co-substituted CaFe_2As_2 further illustrate the similar effects of applied pressure and post - growth annealing and quenching of samples¹⁸ and also underscore the system's pressure sensitivity with $dT_{(AFM/ortho)}/dP \approx -110$ K/kbar and $dT_c/dP \approx -6$ K/kbar.

The aforementioned tunability of CaFe_2As_2 opened the opportunity for studies of the cT phase at ambient pressure (e.g. in FeAs grown CaFe_2As_2 quenched from 960° C), using experimental techniques that are either difficult or impossible to combine with hydrostatic pressure.¹⁹⁻²⁴

^{57}Fe Mössbauer spectroscopy has been widely used to study Fe-As based superconductors and related materials,²⁵⁻²⁹ including Sn-grown CaFe_2As_2 ,^{6,30,31} primarily for probing magnetism. In this work we will use this local probe technique to perform a detailed temperature-dependent study of the cT transition (and the cT phase) in single crystals of 960°C quenched¹⁵ FeAs-grown, pure CaFe_2As_2 , where both the high temperature tetragonal and low temperature cT phases in CaFe_2As_2 are paramagnetic, with no magnetic order. We will compare the results with the available literature data on temperature and pressure induced transition to the cT phase. Some initial ^{57}Fe Mössbauer spectroscopy data on very similar FeAs-grown CaFe_2As_2 crystals with cT ground state were published in Ref. 15 and the pressure induced transition to the cT phase at room temperature in Sn- grown sample was recently studied by Mössbauer spectroscopy in Ref. 32.

The isomer shift and the quadrupole splitting observed in Mössbauer spectroscopy can be directly related to the electron density at the nucleus and the electric field gradient respectively, both of which can be calculated in the framework of *ab-initio* Density Functional Theory. We will employ these calculations in order to provide a theoretical interpretation of the measurements, as well as to predict the As z -coordinates in the 960°C quenched samples.

II. EXPERIMENTAL DETAILS AND COMPUTATIONAL METHODS

CaFe_2As_2 single crystals were grown from ternary melts rich in FeAs, following the procedure described in Ref.¹⁵. The excess liquid was decanted at 960°C , essentially quenching the samples from 960°C to room temperature. The cT transition temperature of the sample was $\sim 90\text{ K}$ as confirmed by dc magnetization measurements (see Fig. 1).¹⁵ In the rest of the paper we will use CaFe_2As_2 to refer to FeAs grown CaFe_2As_2 samples quenched from 960°C to room temperature.

Mössbauer spectroscopy measurements were performed using a SEE Co. conventional constant acceleration type spectrometer in transmission geometry with an $^{57}\text{Co}(\text{Rh})$ source kept at room temperature. The absorber was prepared as a mosaic of 0.04 - 0.1 mm thick single crystals held between two paper disks by a small amount of a pressure sensitive adhesive. The mosaic had the c - axis perpendicular to the disks (with the accuracy of or better than 10°) and arbitrary in-plane orientation. Since CaFe_2As_2 and related materials

are known to be very sensitive to the stresses and strains, including those caused by sample mounting,³³ we performed dc magnetization measurements on a subset of the mosaic with the same mounting as for the Mössbauer measurements (Fig. 1). The cT transition is still sharp, without apparent shift of the transition temperature.

The absorber holder consists of two nested white Delrin cups. The absorber holder was locked in a thermal contact with a copper block with a temperature sensor and a heater, and was aligned with the γ - source and detector. The c -axis of the crystals in the mosaic was parallel to the Mössbauer γ beam. The absorber was cooled to a desired temperature using a Janis model SHI-850-5 closed cycle refrigerator (with vibration damping). The driver velocity was calibrated using an α -Fe foil and all isomer shifts (IS) are quoted relative to the α -Fe foil at room temperature. All the Mössbauer spectra were fitted by the commercial software package MossWinn.³⁴

Ab initio Density Functional Theory (DFT) calculations were performed with the scalar relativistic Full Potential Local Orbital method (FPLO)³⁵. The electric field gradients were obtained according to the technique described in Ref. 36 and implemented in the FPLO code. The Perdew-Burke-Erzenhof³⁷ exchange-correlation potential was employed for all calculations, and we considered $20 \times 20 \times 20$ k-point meshes, with charge density converged within 10^{-8} au^{-3} . In order to calculate the electron density at the location of atomic nuclei, we assumed the model of a finite-size nucleus with constant charge density. Consistency of the calculated electric field gradients and electron densities was verified against values obtained by the Full-Potential Linearized Augmented Plane-Wave method implemented in the WIEN2K code³⁸.

III. RESULTS AND DISCUSSION

The ^{57}Fe Mössbauer spectra of CaFe_2As_2 at selected temperatures between the room temperature and the base temperature of 4.6 K are shown in Fig. 2. At each temperature the spectrum is a quadrupole split doublet with the higher velocity line having almost twice the intensity of the lower velocity line. No secondary phase signal was observed in the spectra. Visually, the temperature induced changes are subtle, but there is a clear, apparent, sharpening of the spectra between room temperature and the base temperature.

Temperature dependent linewidth of the spectra is shown in Fig. 3 a). Overall, it is

almost temperature independent (the linewidth increases by few percent on cooling from room temperature to the base temperature). As has been discussed in Ref. 15, the point symmetry and the location of the Fe site in the ThCr_2Si_2 structure constrains the principal axis of the local electric field gradient tensor to the c - crystalline axis, as a result, a doublet lines intensity ratio of 3 : 1 is expected for the mosaic with the c - axis parallel to the γ beam. Instead, the observed room temperature ratio is $\sim 2.4 : 1$ and it decreases to $\sim 1.95 : 1$ at the base temperature (Fig. 3 (b)). If there is a feature in the behavior around ~ 90 K, it is rather small. The general behavior is consistent with the two temperature points reported earlier.¹⁵ Several possible reasons for the doublet lines intensity ratio being different from 3 : 1 were discussed in Ref. 15.

In Fig. 4 we show the measured isomer shift (IS) which increases upon cooling and has a clear step-like change between 95 K and 85 K. The isomer shift includes contributions from both the chemical shift and the second-order Doppler shift. The latter is known to increase convexly upon decreasing temperature, due to gradual depopulation of the excited phonon states. However, it should be constant at low temperature, because of the quantum mechanical zero-point motion. The chemical shift should not depend on temperature. The main contribution to the temperature dependence of the isomer shift is therefore from the second-order Doppler shift, and is usually described by the Debye model:³⁹

$$\delta(T) = \delta(0) - \frac{9}{2} \frac{k_B T}{Mc} \left(\frac{T}{\Theta_D} \right)^3 \int_0^{\Theta_D/T} \frac{x^3 dx}{e^x - 1}, \quad (1)$$

where c is the velocity of light, M is the mass of the ^{57}Fe nucleus, and $\delta(0)$ is the temperature-independent part. For the isomer shift data in Fig. 4 separate Debye fits, for the tetragonal phase ($T \geq 95$ K) and for the collapsed tetragonal phase ($T \leq 85$ K) were performed. The fits yield $\Theta_D = 239 \pm 16$ K for the high temperature tetragonal phase and $\Theta_D = 316 \pm 7$ K for the low temperature cT phase. These results suggest that the lattice is stiffer in the cT phase.

The relative spectral area (Fig. 5) also shows a distinct step - like feature in the region of the structural transition. The temperature dependence of the relative spectral area in the tetragonal and the cT phase can be analysed within the Debye model.³⁹

$$f = \exp \left\{ \frac{-3E_\gamma^2}{k_B \Theta_D M c^2} \left[\frac{1}{4} + \left(\frac{T}{\Theta_D} \right)^2 \int_0^{\Theta_D/T} \frac{x dx}{e^x - 1} \right] \right\}, \quad (2)$$

where f is the recoilless fraction, which is proportional to the area for thin sample and E_γ is the γ -ray energy. The fits result in the values of the Debye temperature $\Theta_D = 247 \pm 4$ K for the tetragonal phase and $\Theta_D = 266 \pm 11$ K for the cT phase. The inferred Debye temperature values are not far from those obtained in the analysis of the isomer shift. In a similar way, these results suggest that the lattice is stiffer in the cT phase.

Although stiffening of the lattice upon transition to a collapsed tetragonal phase (under pressure) was clearly observed in BaFe_2As_2 ⁴⁰ via compressibility measurements, similar sets^{9,40} of structural data for CaFe_2As_2 appear to be less convincing. However, a detailed study of phonon spectra in CaFe_2As_2 ⁴¹ concluded that the phonons polarized in the ab plane are very similar in the tetragonal and cT phases, whereas transverse acoustic phonons propagating along the c direction stiffen very significantly in the cT phase. These results are consistent with the increase in the Debye temperature in the cT phase as inferred from the temperature dependencies of the isomer shift and the relative spectral area.

Temperature dependent quadrupole splitting (QS) data is presented in Fig. 6. The total change of the QS with temperature is $\sim 25\%$. QS varies strongly in the tetragonal phase and is almost constant in the cT phase. The cT transition is clearly seen as a cusp in QS(T). Qualitatively, this behavior is consistent with the anisotropic thermal expansion of CaFe_2As_2 ²¹: the quadrupole splitting is related to the c/a ratio, that changes considerably above the cT transition and significantly less in the cT phase. In a very general sense this behavior is consistent with the results from the Ref. 32 (with pressure as a control parameter): QS increases on approaching the cT transition, displays a cusp at the transition, and does not change in a significant manner in the cT phase.

In order to better understand the microscopic origin of the observed isomer shift and quadrupole splittings we make use of the definition of the isomer shift δ as given by Ref. 39:

$$\delta = \frac{Ze^2}{5\varepsilon_0} (R_e^2 - R_g^2) [\rho_a(0) - \rho_s(0)] \quad (3)$$

where Z is the nuclear charge, e is the elementary charge, ε_0 is permittivity of vacuum,

R_g and R_e are the nuclear ground and excited state radii and $\rho_s(0)$ and $\rho_a(0)$ are electron densities at the source and absorption nuclei respectively. The only quantity that varies in the measurement is the electron density around the absorption nucleus $\rho_a(0)$ so that we can simply write Eq. (3) as a linear relation

$$\delta = a[\rho_a(0) - b] \quad (4)$$

Note that for ^{57}Fe the constant a is negative^{42–46}. With this taken into account, the observed step-like increase in the isomer shift at the onset of the volume collapse (Fig. 4) would correspond to the likewise drop in the electron density at the iron nucleus. This can be explained as an immediate consequence of charge delocalization brought on by the volume collapse.

The quadrupole splitting Δ can be expressed as³⁹:

$$\Delta = \frac{1}{2}eQV_{zz}\sqrt{1 + \frac{\eta^2}{3}} \quad (5)$$

where Q is the nuclear quadrupole moment, $\eta = |V_{xx} - V_{yy}|/|V_{zz}|$ is the electric field gradient asymmetry, and $|V_{xx}| < |V_{yy}| < |V_{zz}|$ are the eigenvalues of the electric field gradient tensor. Since the sample is tetragonal, the asymmetry η is zero and only V_{zz} is needed.

The crystal structure of the 960° C quenched CaFe_2As_2 sample was characterized in the 5–300 K temperature range by X-ray diffraction measurements¹⁵, however the As z -coordinate positions were not determined. Obtaining the As z -coordinate by structural optimization within DFT may be rather inaccurate due to the unknown nature and distribution of the internal strains within the sample. This leaves us with the option of either using (i) the calculated values of $\rho_a(0)$ and Eq. (4) or (ii) the calculated V_{zz} and Eq. (5) to calibrate the As z -coordinate.

The slope a in Eq. (4) is not accurately known. Values between -0.2 and -0.7 have been reported^{42–46} in the literature. On the other hand, ^{57}Fe nuclear quadrupole moment Q is a well determined quantity with values 0.15–0.17 barn^{45,47–52}. We have thus selected $Q=0.16$ barn and used the measured quadrupole splitting (option (ii) above) to calibrate the As z -coordinates. In order to check for consistency, once the As z -coordinates are obtained as

described above, we can calculate $\rho_a(0)$ with these atomic positions and verify that Eq. (4) is satisfied with a reasonable a value.

In Fig. 7 we show the linear relation between the measured isomer shift in the collapsed tetragonal phase of CaFe_2As_2 and the calculated electron density. The slope is determined to be $a = -0.45 \pm 0.04$ [$\text{au}^3\text{mm/s}$] which is consistent with previously reported values^{43–46}. We note here that Fig. 7 is restricted to the collapsed-tetragonal phase, since in the tetragonal phase the experimentally measured values of the quadrupole splittings cannot be reproduced by the calculations within a reasonable range of As z -coordinate values. We attribute this to the fact that antiferromagnetic fluctuations and electronic correlation effects cannot be accurately captured within DFT. In the collapsed tetragonal phase it has been shown that both correlation effects^{53,54} and antiferromagnetic fluctuations⁵⁵ are suppressed resulting in a good agreement between our DFT calculations and the Mössbauer measurements.

Concentrating now on the tetragonal phase, it is known that relaxing the As z -positions in Fe-based superconductors within DFT is, in general, problematic as has been pointed out in numerous works^{56–58}. However spin polarized calculations within GGA provide reasonable estimates, specially for the orthorhombic phases with long range magnetic order⁵⁷. In order to mimic the effect of electron correlation and antiferromagnetic fluctuations in the tetragonal phase in the framework of DFT, we experimented with spin-polarized GGA calculations with and without on-site Coulomb repulsion. Here we present results with $U=3$ eV and Hund’s coupling $J=1$ eV. We assume Néel order in order to preserve the tetragonal symmetry and account for the antiferromagnetic character of fluctuations. In this way we obtain an estimate of the As z -position in the tetragonal phase which should be taken only as an indication of the general temperature trend. An LDA+DMFT calculation would be more appropriate but it is beyond the scope of the present work.

Figure 8 a) shows the DFT predicted Fe-As bond lengths both in the collapsed tetragonal and the tetragonal phase. Although the predicted bond lengths in the tetragonal phase, as discussed above, can only be considered as a rough estimate, they are consistent with the bond lengths measured under hydrostatic pressure in Sn-grown CaFe_2As_2 samples⁸ and increase with temperature, as expected from thermal expansion measurements.

Interestingly, the Fe-As bond length trend reverses in the collapsed tetragonal phase where it expands as the sample contracts under cooling. Our calculations indicate that this anomaly is key to understand both the structural behavior and the observed quadrupole

splitting in the 960° C quenched sample.

Examination of the behavior of the V_{zz} electric field gradient component for the iron and arsenic nuclei (Fig. 9) in the collapsed tetragonal phase in CaFe_2As_2 shows that each component follows a different trend. While the electric field gradient decreases at the iron nucleus, it increases at the arsenic nucleus as a consequence of the bonding behavior. Relative weakening of the Fe-As bond implies that charge density in the bonding region is reduced, leading to the reduction of the electric field gradient on the iron site. This is reflected in the angular momentum resolved electric field gradient tensor³⁶ which shows a major contributions coming from the $l = 1$ component, implicating reduced hybridization of iron $3d$ orbitals with arsenic $4p$ orbitals as a main culprit leading to the reduction of the electric field gradient. On the other hand, the increase of the electric field gradient at the arsenic site follows from the stronger interlayer As-As bonding as the sample is cooled. This is also reflected in the angular momentum resolved electric field gradient, with $l = 1$ component being essentially the only contribution. Such bond dynamics indicates that some of the charge in the Fe-As bond region is transferred to the interlayer As-As bond region, contributing to its strength and helping to stabilize the collapsed tetragonal phase at ambient pressure.

In Fig. 8 b) the predicted interlayer As-As to Fe-As bond length ratio for the 960° C quenched sample at ambient pressure and the measured values for Sn-grown CaFe_2As_2 samples under 0.63 GPa below 250 K⁸ are shown. We observe that the Fe-As bonds appear to be relatively shorter in the tetragonal phase of the 960° C quenched sample. Such bond configuration can lead to charge saturation in the Fe-As bond region under thermal contraction. At a certain temperature it becomes energetically more favorable to transfer some of the charge into the interlayer As-As bond region, precipitating the formation of the interlayer As-As bond which in turn stabilizes the collapsed tetragonal phase. This dynamic continues in the collapsed tetragonal phase, where the Fe-As bond keeps getting weaker while the interlayer As-As bond gets stronger until zero temperature is reached, where the bond lengths revert to the ratio observed in the Sn-grown samples under hydrostatic pressure.

IV. SUMMARY

Experimentally clear features in the temperature dependencies of the isomer shift, relative spectral area and quadrupole splitting are observed at the transition from tetragonal to cT

phase in CaFe_2As_2 . From the temperature dependent isomer shift and spectral area data, an average stiffening of the phonon modes in the cT phase is inferred. Quadrupole splitting increases by $\sim 25\%$ on cooling from room temperature to the cT transition, in agreement with a large anisotropy of thermal expansion in this temperature region.

Additionally, we performed *ab initio* density functional theory calculations of the electric field gradient and the electron density of CaFe_2As_2 in the tetragonal and collapsed tetragonal phase. Comparison of these calculations to the measurements allows for the determination of the As z -positions in the 960°C quenched sample. The resulting bond lengths are consistent with the data recorded for Sn-grown samples under hydrostatic pressure. In the collapsed tetragonal phase we also find a good agreement of the slope of the measured isomer shift versus the calculated electron density with previously reported values for other iron compounds.

In the tetragonal phase, as the sample is cooled, the Fe-As bonds undergo thermal contraction, resulting in larger electric field gradients at the iron nuclei and leading to an increase of the quadrupole splitting. In the collapsed tetragonal phase we observe instead an anomalous behavior of the Fe-As bond, whereby it undergoes expansion as the sample is cooled, resulting in a decrease of the observed quadrupole splitting. We attribute this behavior to charge redistribution from the Fe-As bond region into the interlayer As-As region, resulting in stabilization of the collapsed tetragonal phase. In our proposed scenario, it is annealing which stabilizes relatively shorter Fe-As bonds, leading to charge saturation of the Fe-As bond region as the sample contracts.

ACKNOWLEDGMENTS

X.M. was supported in part by the China Scholarship Council. Work at the Ames Laboratory was supported by the US Department of Energy, Basic Energy Sciences, Division of Materials Sciences and Engineering under Contract No. DE-AC02-07CH11358. M.T. and R.V. acknowledge financial support by the DFG (Deutsche Forschungsgemeinschaft) through grant SPP 1458.

* Currently at the Department of Physics, University of California - San Diego

- ¹ N. Ni, S. Nandi, A. Kreyssig, A. I. Goldman, E. D. Mun, S. L. Bud'ko, and P. C. Canfield, *Phys. Rev. B* **78**, 014523 (2008).
- ² A. I. Goldman, D. N. Argyriou, B. Ouladdiaf, T. Chatterji, A. Kreyssig, S. Nandi, N. Ni, S. L. Bud'ko, P. C. Canfield, and R. J. McQueeney, *Phys. Rev. B* **78**, 100506 (2008).
- ³ G. Wu, H. Chen, T. Wu, Y. L. Xie, Y. J. Yan, R. H. Liu, X. F. Wang, J. J. Ying, and X. H. Chen, *J. Phys. Condens. Matter* **20**, 422201 (2008).
- ⁴ F. Ronning, T. Klimczuk, E. D. Bauer, H. Volz, and J. D. Thompson, *J. Phys. Condens. Matter* **20**, 322201 (2008).
- ⁵ P. C. Canfield, S. L. Bud'ko, N. Ni, A. Kreyssig, A. I. Goldman, R. J. McQueeney, M. S. Torikachvili, D. N. Argyriou, G. Luke, and W. Yu, *Physica C* **469**, 404 (2009).
- ⁶ M. Alzamora, J. Munevar, E. Baggio-Saitovitch, S. L. Bud'ko, Ni Ni, P. C. Canfield, and D. R. Sánchez, *J. Phys. Condens. Matter* **23**, 145701 (2011).
- ⁷ Milton S. Torikachvili, Sergey L. Bud'ko, Ni Ni, and Paul C. Canfield, *Phys. Rev. Lett.* **101**, 057006 (2008).
- ⁸ A. Kreyssig, M. A. Green, Y. Lee, G. D. Samolyuk, P. Zajdel, J. W. Lynn, S. L. Bud'ko, M. S. Torikachvili, N. Ni, S. Nandi, J. B. Leão, S. J. Poulton, D. N. Argyriou, B. N. Harmon, R. J. McQueeney, P. C. Canfield, and A. I. Goldman, *Phys. Rev. B* **78**, 184517 (2008).
- ⁹ A. I. Goldman, A. Kreyssig, K. Prokeš, D. K. Pratt, D. N. Argyriou, J. W. Lynn, S. Nandi, S. A. J. Kimber, Y. Chen, Y. B. Lee, G. Samolyuk, J. B. Leão, S. J. Poulton, S. L. Bud'ko, N. Ni, P. C. Canfield, B. N. Harmon, and R. J. McQueeney, *Phys. Rev. B* **79**, 024513 (2009).
- ¹⁰ W. Yu, A. A. Aczel, T. J. Williams, S. L. Bud'ko, N. Ni, P. C. Canfield, and G. M. Luke, *Phys. Rev. B* **79**, 020511 (2009).
- ¹¹ Hanoh Lee, Eunsung Park, Tuson Park, V. A. Sidorov, F. Ronning, and E. D. Bauer, and J. D. Thompson, *Phys. Rev. B* **80**, 024519 (2009).
- ¹² Sergey L. Bud'ko, Ni Ni, and Paul C. Canfield, *Philos. Mag.* **90**, 1219 (2010).
- ¹³ M. S. Torikachvili, S. L. Bud'ko, N. Ni, P. C. Canfield, and S. T. Hannahs, *Phys. Rev. B* **80**, 014521 (2009).
- ¹⁴ K. Prokes, A. Kreyssig, B. Ouladdiaf, D. K. Pratt, N. Ni, S. L. Bud'ko, P. C. Canfield, R. J. McQueeney, D. N. Argyriou, and A. I. Goldman, *Phys. Rev. B* **81**, 180506 (2010).
- ¹⁵ S. Ran, S. L. Bud'ko, D. K. Pratt, A. Kreyssig, M. G. Kim, M. J. Kramer, D. H. Ryan, W. N. Rowan-Weetaluktuk, Y. Furukawa, B. Roy, A. I. Goldman, and P. C. Canfield, *Phys. Rev. B*

- 83**, 144517 (2011).
- ¹⁶ S. Ran, S. L. Bud'ko, W. E. Straszheim, J. Soh, M. G. Kim, A. Kreyssig, A. I. Goldman, and P. C. Canfield, Phys. Rev. B **85**, 224528 (2012).
 - ¹⁷ S. Ran, S. L. Bud'ko, W. E. Straszheim, and P. C. Canfield, Phys. Rev. B **90**, 054501 (2014).
 - ¹⁸ E. Gati, S. Köhler, D. Guterding, B. Wolf, S. Knöner, S. Ran, S. L. Bud'ko, P. C. Canfield, and M. Lang, Phys. Rev. B **86**, 220511 (2012).
 - ¹⁹ J. H. Soh, G. S. Tucker, D. K. Pratt, D. L. Abernathy, M. B. Stone, S. Ran, S. L. Bud'ko, P. C. Canfield, A. Kreyssig, R. J. McQueeney, and A. I. Goldman, Phys. Rev. Lett. **111**, 227002 (2013).
 - ²⁰ Y. Furukawa, B. Roy, S. Ran, S. L. Bud'ko, and P. C. Canfield, Phys. Rev. B **89**, 121109 (2014).
 - ²¹ Sergey L. Bud'ko, Sheng Ran, and Paul C. Canfield, Phys. Rev. B **88**, 064513 (2013).
 - ²² R. S. Dhaka, Rui Jiang, S. Ran, S. L. Bud'ko, P. C. Canfield, B. N. Harmon, Adam Kaminski, Milan Tomić, Roser Valení, and Yongbin Lee, Phys. Rev. B **89**, 020511 (2014).
 - ²³ K. Gofryk, B. Saproov, T. Durakiewicz, A. Chikina, S. Danzenbächer, D. V. Vyalikh, M. J. Graf, and A. S. Sefat, Phys. Rev. Lett. **112**, 186401 (2014).
 - ²⁴ Bayrammurad Saproov, Claudia Cantoni, Minghu Pan, Thomas C. Hogan, William Ratcliff II, Stephen D. Wilson, Katharina Fritsch, Bruce D. Gaulin, and Athena S. Sefat Sci. Rep. **4**, 4120 (2014).
 - ²⁵ Marianne Rotter, Marcus Tegel, Dirk Johrendt, Inga Schellenberg, Wilfried Hermes, and Rainer Pöttgen, Phys. Rev. B **78**, 020503 (2008).
 - ²⁶ Israel Nowik, Israel Felner, Physica C **469**, 485 (2009).
 - ²⁷ I. Nowik, I. Felner, Z. Ren, Z. A. Xu, and G. H. Cao, J. Phys.: Conf. Ser. **217**, 012121 (2010).
 - ²⁸ Amar Nath and Airat Khasanov, in: *Mossbauer Spectroscopy: Applications in Chemistry, Biology, and Nanotechnology*, edited by Virender K. Sharma, Gostar Klingelhofer, and Tetsuaki Nishida, John Wiley & Sons, Inc. (2013) p. 535.
 - ²⁹ A. K. Jasek, K. Komędera, A. Błachowski, K. Ruebenbauer, J. Żukrowski, Z. Bukowski, and J. Karpinski, Philos. Mag. **95**, 493 (2015).
 - ³⁰ Neeraj Kumar, R. Nagalakshmi, R. Kulkarni, P. L. Paulose, A. K. Nigam, S. K. Dhar, and A. Thamizhavel, Phys. Rev. B **79**, 012504 (2009).
 - ³¹ Zhiwei Li, Xiaoming Ma, Hua Pang, and Fashen Li, J. Phys. Condens. Matter **23**, 255701 (2011).

- ³² Yui Sakaguchi, Shugo Ikeda, Tetsuji Kuse and Hisao Kobayashi, J. Phys. Condens. Matter **26**, 295702 (2014).
- ³³ Sheng Ran, *Combined effects of post-growth thermal treatment and chemical substitution on physical properties of CaFe_2As_2* , Ph. D. Thesis, Iowa State Universty (2014).
- ³⁴ Z. Klencsár, MossWinn 3.0i xp Manual (1995-2009).
- ³⁵ K. Koepnik and H. Eschrig, Phys. Rev. B **59**, 1743 (1999).
- ³⁶ K. Koch, K. Koepnik, D. V. Neck, H. Rosner and S. Cottenier, Phys. Rev. B **81** 032507 (2010).
- ³⁷ J. P. Perdew, K. Burke and M. Ernzerhof, Phys. Rev. Lett. **77**, 3865 (1996).
- ³⁸ P. Blaha, K. Schwarz, G. K. H. Madsen, D. Kvasnicka, and J. Luitz, An Augmented Plane Wave Plus Local Orbitals Program for Calculating Crystal Properties (Karlheinz Schwarz, Techn. Universität Wien, Austria) (2001).
- ³⁹ N.N. Greenwood and T.C. Gibb., *Mössbauer Spectroscopy*, (Chapman and Hall Ltd, London) (1971)
- ⁴⁰ R. Mittal, S. K. Mishra, S. L. Chaplot, S. V. Ovsyannikov, E. Greenberg, D. M. Trots, L. Dubrovinsky, Y. Su, Th. Brueckel, S. Matsuishi, H. Hosono, and G. Garbarino, Phys. Rev. B **83**, 054503 (2011).
- ⁴¹ R. Mittal, R. Heid, A. Bosak, T. R. Forrest, S. L. Chaplot, D. Lamago, D. Reznik, K.-P. Bohnen, Y. Su, N. Kumar, S. K. Dhar, A. Thamizhavel, Ch. Rüegg, M. Krisch, D. F. McMorrow, Th. Brueckel, and L. Pintschovius, Phys. Rev. B **81**, 144502 (2010).
- ⁴² O. Eriksson and A. Svane, J. Phys.: Cond. Mat. **1**, 1589 (1989).
- ⁴³ T. Lovell, W.-G. Han, T. Liu and L. Noodleman, J. Am. Chem. Soc. **124** 5890 (2002)
- ⁴⁴ F. Neese, Inorg. Chim. Acta **337**, 181 (2002)
- ⁴⁵ S. Sinnecker, L. D. Slep, E. Bill and F. Neese, Inorg. Chem. **44**, 2245 (2005)
- ⁴⁶ W.-G. Han, T. Liu and T. Lovell, L. Noodleman, J. Comput. Chem. **27**, 1292 (2006)
- ⁴⁷ S. Lauer, V. R. Marathe and A. Trautwein, Phys. Rev. A **19**, 1852 (1979)
- ⁴⁸ P. Dufek, P. Blaha and K. Schwarz, Phys. Rev. Lett. **75**, 3545 (1995)
- ⁴⁹ G. Martínez-Pinedo, P. Schwerdtfeger, E. Caurier, K. Langanke, W. Nazarewicz and T. Söhnel, Phys. Rev. Lett. **87**, 062701 (2001)
- ⁵⁰ Y. Zhang, W. Gossman and E. Oldfield, J. Am. Chem. Soc. **125**, 16387 (2003)
- ⁵¹ Y. Zhang and E. Oldfield, J. Phys. Chem. **107**, 4147 (2003)

- ⁵² Z. Zhi, D. Guenzburger and D. E. Ellis, J. Theo. Chem. **678**, 145 (2004)
- ⁵³ Jean Diehl, Steffen Backes, Daniel Guterding, Harald O. Jeschke, and Roser Valentí, Phys. Rev. B **90**, 085110 (2014)
- ⁵⁴ Subhasish Mandal, R. E. Cohen, and K. Haule, Phys. Rev. B **90**, 060501(R) (2014)
- ⁵⁵ D. K. Pratt, Y. Zhao, S. A. J. Kimber, A. Hiess, D. N. Argyriou, C. Broholm, A. Kreyssig, S. Nandi, S. L. Bud'ko, N. Ni, P. C. Canfield, R. J. McQueeney, and A. I. Goldman, Phys. Rev. B **79**, 060510(R) (2009)
- ⁵⁶ Z. P. Yin, S. Lebégue, M. J. Han, B. P. Neal, S. Y. Savrasov, and W. E. Pickett, Phys. Rev. Lett. **101**, 047001 (2008)
- ⁵⁷ I. I. Mazin, M. D. Johannes, L. Boeri, K. Koepernik, and D. J. Singh, Phys. Rev. B **78**, 085104 (2008)
- ⁵⁸ Markus Aichhorn, Leonid Pourovskii, and Antoine Georges, Phys. Rev. B **84**, 054529 (2011)

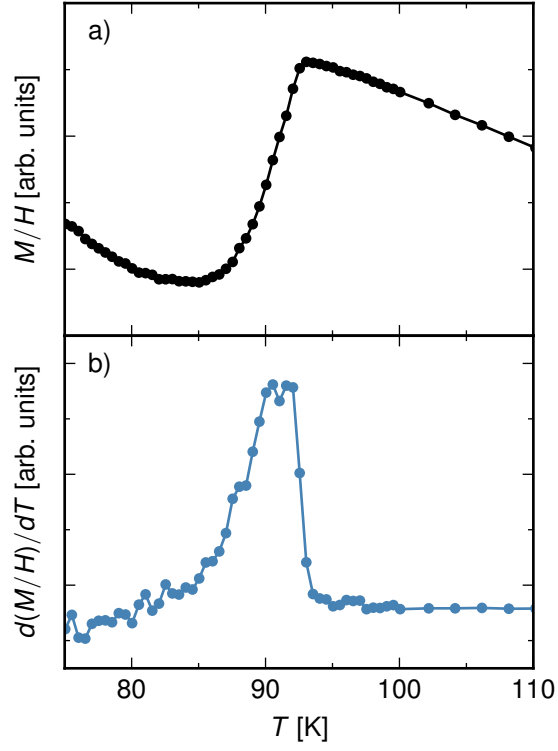


FIG. 1. Temperature dependent magnetization, $M/H(T)$ and its temperature derivative, $d(M/H)/dT$, of a part of CaFe_2As_2 crystals mosaic used for Mössbauer measurements in a vicinity of the cT transition. Note that the paper and adhesive of the mount give some small, weakly temperature dependent contribution to $M/H(T)$.

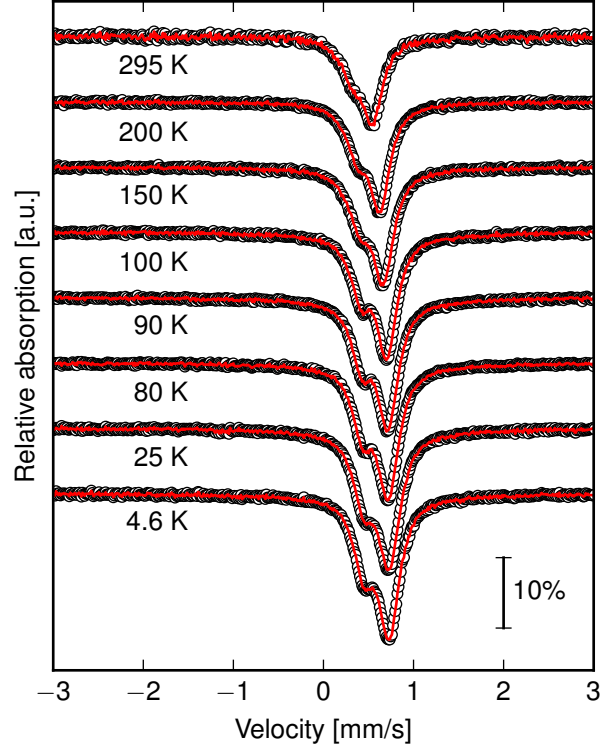


FIG. 2. (Color online) ^{57}Fe Mössbauer spectra of CaFe_2As_2 at selected temperatures. Symbols - data, lines - fits. $T_{cT} \sim 90$ K, as shown in Fig. 1.

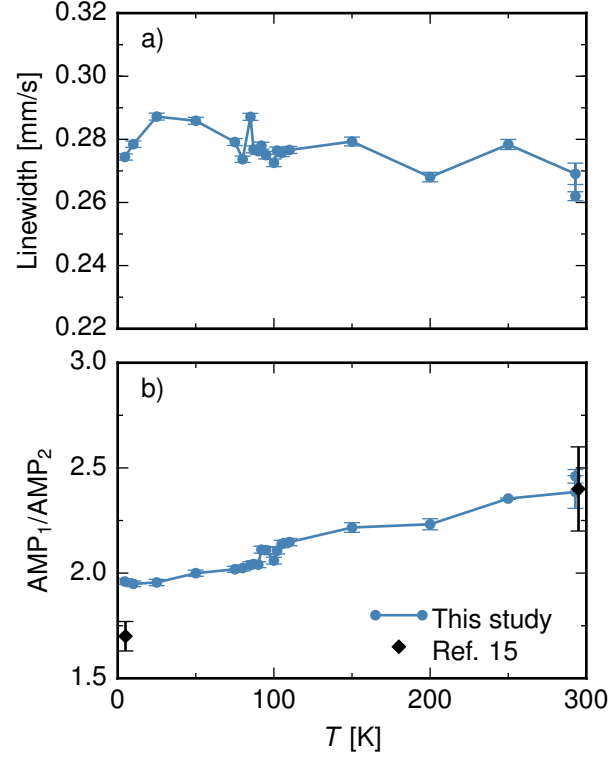


FIG. 3. (Color online) (a) Temperature dependence of the linewidth; (b) The intensity ratio of the doublet lines as a function of temperature. Circles - this work, rhombuses - Ref. 15.

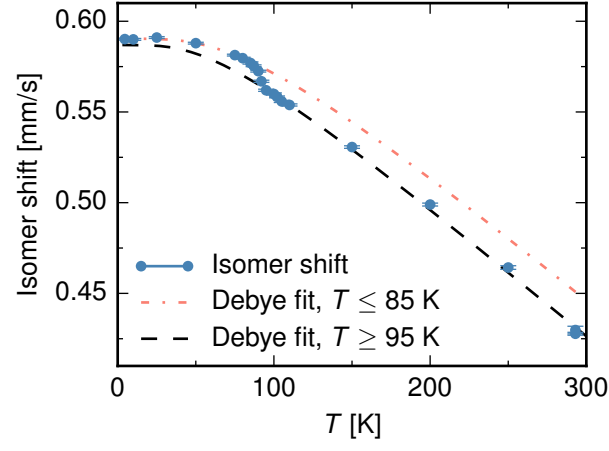


FIG. 4. (Color online) Temperature dependent isomer shift of CaFe_2As_2 . Dashed line - Debye fit for $T \geq 95$ K resulting in $\Theta_D = 239 \pm 16$ K, dash-dotted line Debye fit for $T \leq 85$ K resulting in $\Theta_D = 316 \pm 7$ K

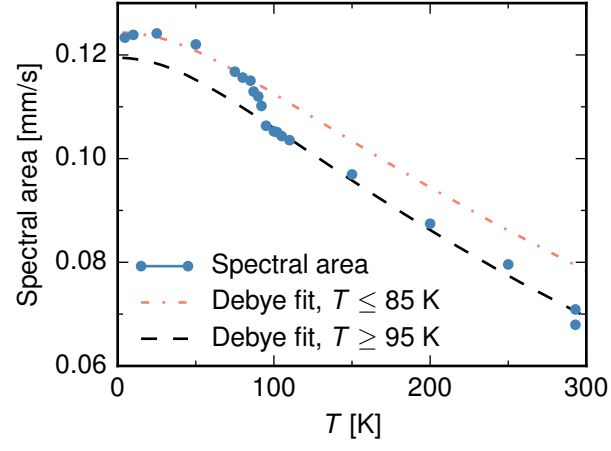


FIG. 5. (Color online) Temperature dependent relative spectral area of CaFe_2As_2 . Dashed line - Debye fit for $T \geq 95$ K resulting in $\Theta_D = 247 \pm 4$ K, dash-dotted line Debye fit for $T \leq 85$ K resulting in $\Theta_D = 266 \pm 11$ K

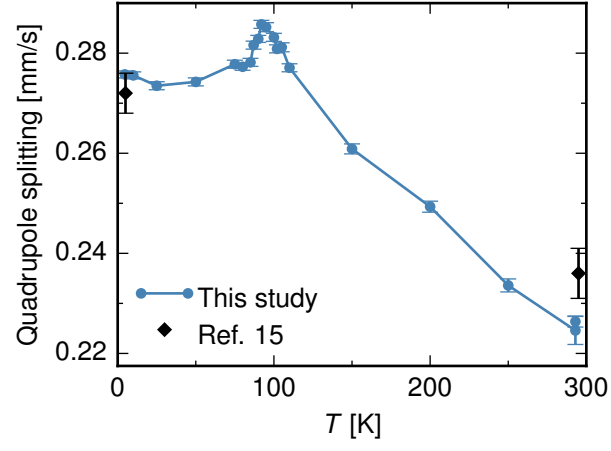


FIG. 6. (Color online) Temperature dependent quadrupole splitting of CaFe_2As_2 . Circles - this work, rhombuses - Ref. 15.

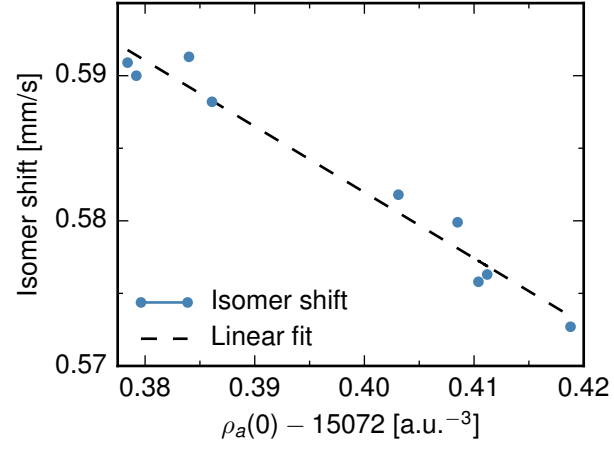


FIG. 7. (Color online) The linear relationship between the calculated charge density at the iron nucleus and the measured isomer shift in the collapsed-tetragonal phase.

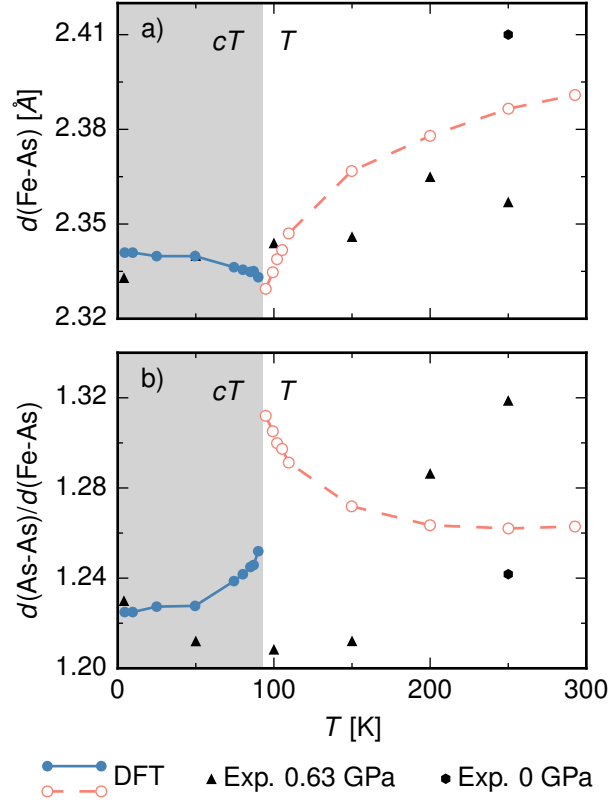


FIG. 8. (Color online) (a) The *ab-initio* predicted Fe-As bond length in the 960° C quenched sample compared against the measured bond lengths on Sn-grown samples under pressure⁸. (b) Predicted interlayer to As-As to Fe-As bond ratio in the 960° C quenched sample compared against the Sn-grown samples⁸. Note that the shaded region denotes the collapsed-tetragonal phase, and that the predicted bond lengths shown in the tetragonal phase (outside the shaded region) can only be taken as a rough estimate.

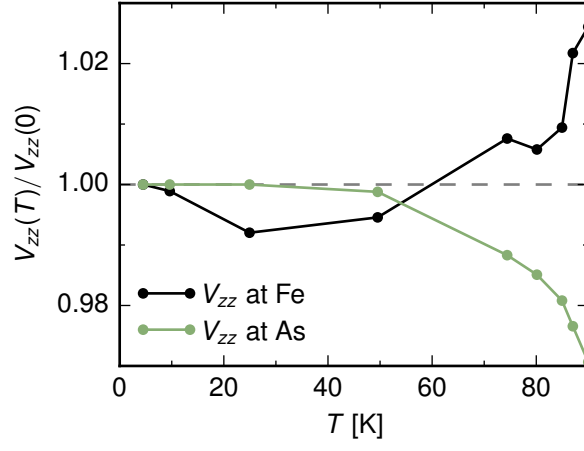


FIG. 9. (Color online) The calculated V_{zz} component of the electric field gradient for the iron and arsenic sites normalized to their respective zero temperature values.